Low Temperature Crystallization Enables 21.9% Efficient Single-Crystal $MAPbI_3$ Inverted Perovskite Solar Cells

Abdullah Y. Alsalloum,[†,‖] Bekir Turedi,[†,‖] Xiaopeng Zheng,[†] Somak Mitra,[†] Ayan A. Zhumekenov, [†] Kwang Jae Lee,[†] Partha Maity,[†] Issam Gereige[‡], Ahmed AlSaggaf[‡], Iman S. Roqan,[†] Omar F. Mohammed,[*,†] and Osman M. Bakr[*,†]

[†]Division of Physical Sciences and Engineering, King Abdullah University of Science and Technology, Thuwal 23955-6900, Kingdom of Saudi Arabia

[‡]Saudi Aramco Research & Development Center, Dhahran 31311, Kingdom of Saudi Arabia

Corresponding Authors:

*E-mail: omar.abdelsaboor@kaust.edu.sa

*E-mail: osman.bakr@kaust.edu.sa

Author Contributions: ‖ Abdullah Y. Alsalloum and Bekir Turedi contributed equally to this work.

Abstract

Lead halide perovskite solar cells (PSCs) have advanced rapidly in performance over the past decade. Single-crystal PSCs based on microns-thick grain-boundary-free films with long charge carrier diffusion lengths and enhanced light absorption (relative to polycrystalline films) have recently emerged as candidates for advancing PSCs further toward their theoretical limit. Thus far, the preferred method to grow $MAPbI_3$ single-crystal films for PSCs involves solution-processing at temperatures ≳120 °C, which adversely affects the films' crystalline quality, especially at the surface, primarily due to methylammonium iodide loss at such high temperatures. Here we devise a solvent-engineering approach to reduce the crystallization temperature of $MAPbI_3$ single-crystal films (<90 °C), yielding better quality films with longer carrier lifetimes. Single-crystal inverted PSCs fabricated with this strategy show markedly enhanced open-circuit voltages (1.15 V vs. 1.08 V for controls), leading to power conversion efficiencies of up to 21.9%, which are among the highest reported for $MAPbI_3$-based devices.

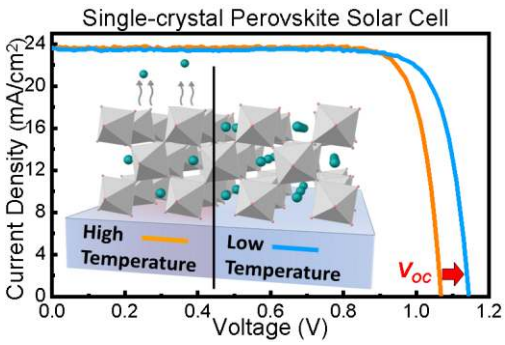

Lead halide perovskite solar cells (PSCs) are the fastest growing photovoltaic technology to date, reaching commercially compelling power conversion efficiencies (PCEs) in just under a decade of development.[1] PSCs are mainly based on polycrystalline thin films (≲700 nm), where grain boundaries and very rapid crystallization give rise to bulk and surface defects that hinder the further development of their optoelectronic performance.[2] As such, mitigating electronic defects, particularly those stemming from surfaces and grain-boundaries, has become a central theme of perovskite research.[3–12] On the other hand, in conventional state-of-the-art semiconductors such as Si and GaAs, record performing devices rely on single-crystalline absorbers possessing very low defect concentrations.[13–15] Perovskite single-crystals were also shown to have extremely low trap-state densities, resulting in carrier diffusion lengths that are about two orders of magnitude longer than those in their polycrystalline analogues.[16–22] Such long diffusion lengths, afford the utilization of relatively thick single-crystal films (~20 microns) as solar cell absorbers.[23] Thick films enable the perovskite absorber layer to practically extend its light absorption further into the Near-IR spectrum, due to the increasing cross-section of the indirect bandgap as film thicknesses increase (note: the bandgap of $MAPbI_3$ has an indirect-direct nature; the indirect bandgap is situated on the lower energy side of the direct bandgap, but has a lower absorption coefficient).[24–26] Therefore, single-crystal PSCs (SC-PSCs) offer an opportunity to improve upon the absorption of polycrystalline films, which is a necessary step for bridging the efficiency gap between PSCs and

the theoretical Shockley-Queisser efficiency limit for single-junction solar cells.[27,28] However, in contrast to the multitude of facile approaches to fabricating high efficiency polycrystalline film PSCs, the options for growing single-crystals suitable for PSCs are limited and so far only one report has demonstrated SC-PSCs with PCEs >20%.[23]

Recently, we showcased the potential of SC-PSCs by realizing ~21.1% efficient devices based on ~20 μm-thick methylammonium lead iodide ($MAPbI_3$, where $MA=CH_3NH_3$) monocrystalline absorber films.[23] In an inert environment, the crystal films were grown directly on the hole transporting layer using a solution space-limited inverse-temperature crystal (ITC) growth method[29,30] — considered the most common single-crystal growth technique for lead halide perovskites — wherein $MAPbI_3$ was dissolved in γ-butyrolactone (GBL) as the solvent, and the temperature was raised to ~120 °C for nucleation and growth. Unfortunately, the requirement of processing at such a high temperature (set by the solubility of $MAPbI_3$ in GBL) inevitably leads to the deterioration of the crystal quality, especially at the surface, given the hybrid soft ionic nature of $MAPbI_3$ and volatility of the organic cation.[31–35] Moreover, the problem is exacerbated by the fact that longer hours are needed for thin film crystal growth due to the limited diffusion of the solution in thin confined spaces. The thermally-triggered instability is initiated at the surface, whereby the loss of methylammonium iodide (MAI) leads to a layer-by-layer degradation, leaving behind a lead iodide (PbI_2) rich surface.[31] While surface defects might not have a profound effect on the short-circuit current (J_{SC}) due to the eventual escape of a portion of the trapped charges toward the collecting electrodes, they would significantly affect the open-circuit voltage (V_{OC}).[5,35]

Here, we designed an approach that enables the growth of $MAPbI_3$ single-crystal thin films to occur at lower temperatures, and, thereby, limiting the escape of MAI from the crystal structure (Figure 1a, 1b). We optimized a solvent mixture of propylene carbonate (PC) and gamma-

butyrolactone (GBL) such that low-temperature (<90 ºC) ITC of $MAPbI_3$ thin films on the hole transporting layer is feasible. SC-PSCs fabricated with this low-temperature crystallization strategy show a significant enhancement in the open-circuit voltage (V_{OC}) with values as high as 1.15 V (vs. 1.08 V for control devices), leading to PCEs of up to 21.9%. These results highlight the potential of SC-PSCs in advancing perovskite photovoltaic technology, and emphasize the room for further performance improvement by enhancing the surface properties.

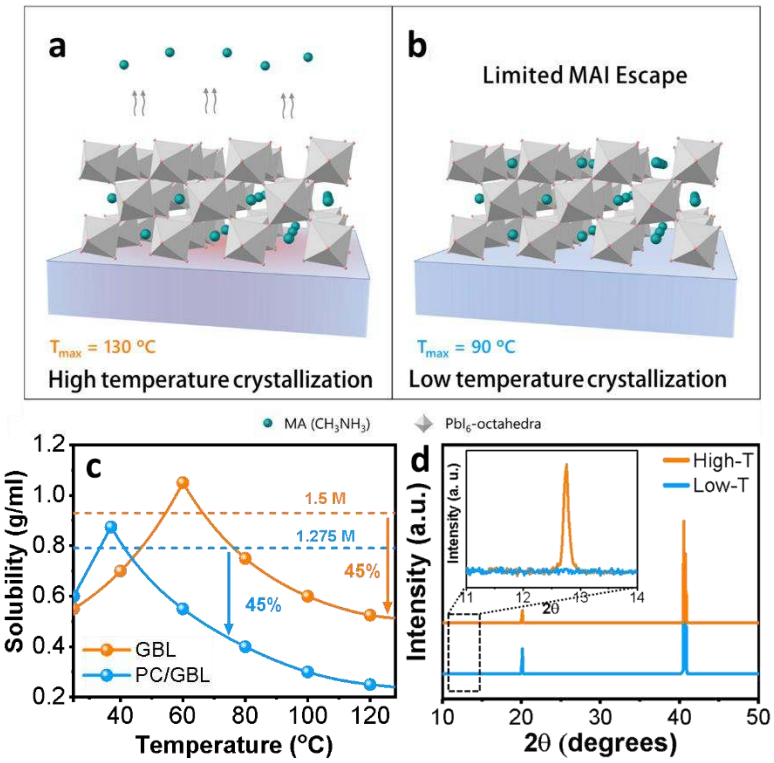

Figure 1. Schematic illustration of methylammonium iodide escape from $MAPbI_3$ single-crystal films at **(a)** high temperature (High-T) and **(b)** low temperature (Low-T) crystallization. **(c)** Temperature-dependent solubility of $MAPbI_3$ in GBL and PC/GBL solvent mixture. **(d)** XRD 2θ patterns of the single-crystal thin films grown at high and low temperatures.

Figure 1c shows the temperature-dependent solubility of $MAPbI_3$ in GBL and PC/GBL solvent mixture (see Supplementary Information for further details). In GBL, the solubility is maximum at around 60 °C and can sustain a concentration of about 1.7 M before precipitating. A lower concentration is normally chosen (~1.5M) when growing thin single-crystal films, since complete dissolution of the precursors is ensured and precipitation from slight temperature changes is prevented when transferring the solution to the substrate. As the temperature increases, nucleation occurs at ~100 °C. To obtain larger crystals suitable for solar cell fabrication, the temperature is further raised to a maximum of ~130 °C. To lower the crystallization temperature and improve the yield, the solubility curve needs to be shifted (horizontally in Figure 1c) to lower temperatures while the final solubility at the crystallization temperature needs to be decreased (vertically in Figure 1c) without substantially sacrificing the initial solubility at the precursor preparation temperature. In other words, the solubility of the perovskite in GBL should be lowered while preserving ITC. We found that adding the solvent PC lowers the crystallization temperature resulting in higher yields without dissolving the hole transporting layer poly(triaryl amine) (PTAA) in which the solution makes direct contact with during crystallization. PC on its own also shows ITC of $MAPbI_3$[36]; however, the solubility of $MAPbI_3$ in PC is very low to be adopted for thin single-crystal growth with a maximum solubility of around 0.45M measured at room temperature. Adding 35% by volume of PC to GBL is sufficient to modify the curve such that the solubility is maximum at ~37°C. In this case, nucleation happens at ~60°C and the temperature can be increased to ~90°C for further crystal growth. Lowering the crystallization temperature further is possible, but creates difficulties in obtaining decent crystal areas suitable for solar cell fabrication as thermal convection of the micrometer-confined solution becomes restricted, leading to many nucleation sites occurring in response to minor temperature changes. It is worth noting

that there are existing methods that utilize low-temperature growth to produce large high quality bulk $MAPbI_3$ crystals such as the antisolvent vapor-assisted crystallization method (AVC) at room temperature and cooling from a hydroiodic acid solution (<75 °C).[16,17,37] However, such techniques are incompatible with the space-limited thin film growth method adopted to fabricate efficient solar cells. Common antisolvents such as toluene and dichloromethane (DCM) cannot substitute for PC, as they readily dissolve PTAA and are volatile. Moreover, the use of acids such as hydroiodic acid (HI) and formic acid was avoided as they alter the substrate properties when in contact for a prolonged period of time.[38]

We compared the conventional single-crystal films grown at high temperatures (100 °C - 130 °C) in GBL to single-crystal films grown using our new approach at lower temperatures (60 °C - 90 °C). X-ray diffraction (XRD) shows clear evidence for the escape of MAI from the crystal surface in the former case. While, a full range XRD scan (Figure 1d) shows no discernible differences between the patterns of single-crystal thin films obtained at low and high temperatures, a zoom-in extended scan of the region corresponding to PbI_2 (Inset Figure 1d), reveals an obvious peak emerging at 12.7° for the high-temperature grown sample, whereas the low-temperature one displays no peak within the detection limit of the instrument.

To further assess the surface quality, the charge carrier recombination dynamics were explored on crystal films grown on glass to analyze the intrinsic material response without the influence of external factors. Time-resolved photoluminescence (TRPL) lifetime measurements were performed on these samples upon 385-nm excitation. The average carrier lifetime in the low-temperature-grown film is much longer (164 ns) than that of the high-temperature film (42 ns), as illustrated in Figure 2a. The longer lifetime in the low-temperature grown film indicates that the surface possesses less defect states and crystalline disorder as compared to the high-temperature

grown sample.[39] The steady-state photoluminescence (PL) (Figure 2b) reveals close to a 3-fold increase in PL intensity emanating from the low-temperature grown film which is consistent with the PL lifetime data, a strong indication for the reduction in the number of non-radiative recombination centers.[35] To confirm the uniformity of the increased PL, two-dimensional (2D) contour mapping of the PL intensity was carried out. Figure 2c and 2d show that the increase in PL is consistent and independent of the location on the crystal's surface. The disparity in PL intensity for both thin crystal samples reveals that crystallizing at a lower temperature enhances radiative recombination channels as compared to higher temperature growth.

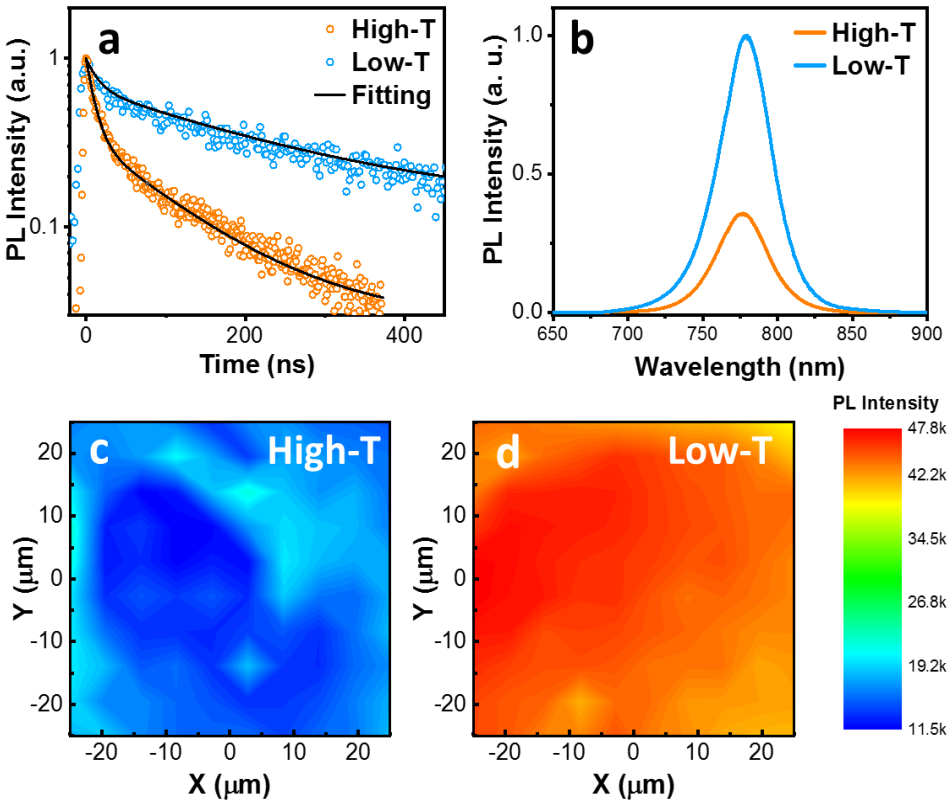

Figure 2. Optical Characterization. **(a)** TRPL, **(b)** steady-state PL spectra, and PL mapping comparisons of the $MAPbI_3$ single-crystal films grown at **(c)** High-T and **(d)** Low-T.

To investigate the photovoltaic performance of the grown films, inverted (p-i-n junction) planar SC-PSCs were fabricated and tested under 1-sun illumination. A top-view scanning electron microscopy (SEM) image of the crystal film (Figure S1) shows a smooth grain-boundary-free surface, which allows for the complete and even coverage of the transporting layers and electrode. The cross-sectional SEM images of the cells (Figure 3a, b) reveal a ~20 μm smooth monocrystalline film. The device configuration is: ITO/PTAA/$MAPbI_3$ single-crystal/C60/Bathocuproine (BCP)/Cu (Figure 3c). Figure 3d compares the reverse-scan *J-V* curves of the best devices fabricated for single-crystal films grown by both techniques. Although the short-circuit current (J_{SC}) and fill factor (*FF*) are similar in both cases, the V_{OC} of the device fabricated with the low-temperature approach (1.144 V) was markedly higher than the V_{OC} of the device fabricated in the high-temperature regime (1.067 V). This increase in V_{OC} is responsible for the better photovoltaic performance. To better identify the trends and assess the reproducibility of the two techniques, a statistical analysis of 10 different cells of each was carried out. The corresponding photovoltaic parameters are illustrated in Figure 3e-3h displaying good reproducibility of the fabricated devices. The low-and high-temperature approaches yield maximum V_{OC} values of 1.15 V and 1.08 V, and average values of 1.13 V and 1.06 V, respectively. The J_{SC} and *FF* are largely unaffected. This improved V_{OC} is reminiscent of the one achieved in polycrystalline PSCs after defect passivation treatments.[40–42] Crystallographic defects trap charges and promote non-radiative recombination, which, in turn, restrains the quasi-Fermi level splitting leading to suppression of the photovoltage.[43–45] Consequently, a superior V_{OC} is observed in the lower temperature grown films with better crystal quality. It is well established in the literature that the surface of perovskite single crystals lags significantly behind their bulk in terms of charge traps, rendering the surface a major limiting factor in optoelectronic performance of single

crystals.[33,37] Stolterfoht et al. have shown that an improvement in the bulk lifetime would unlikely lead to a V_{OC} enhancement when the surface quality is poor.[46,47] This along with the observed sensitivity of $MAPbI_3$ to high temperatures and the fact that thin single crystal films possess a much higher surface area to volume ratio than bulk crystals (aspect ratio of about 100:1) have led us to focus our analysis on the surface; however, we do not exclude a quality improvement in the thin crystal bulk as a result of lower temperature growth.

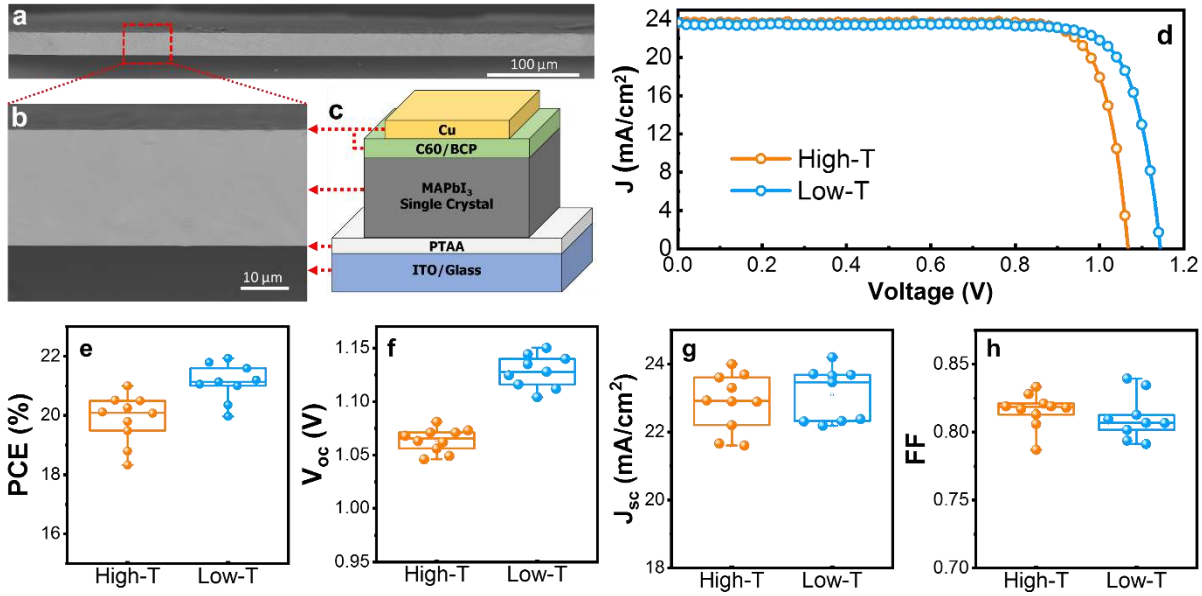

Figure 3. Characterization of perovskite single-crystal solar cells. **(a)** and **(b)** Cross-sectional SEM images of the single-crystal device. Note that the few nanometer-thick transporting layers are not visible at such magnifications. **(c)** Device structure of the single-crystal solar cells. **(d)** *J–V* curves comparison of the best SC-PSCs made from High-T and Low-T crystallization. Statistical comparison of the photovoltaic parameters for 10 devices including **(e)** power conversion efficiency (PCE), **(f)** open circuit voltage (V_{OC}), **(g)** short circuit current (J_{SC}), and **(h)** fill factor (*FF*). All data was measured under 1-sun illumination.

Figure 4a shows the *J-V* characteristics of the champion device. The reverse-scan displays a V_{OC}, J_{SC} and *FF* of 1.144 V, 23.68 mA cm^{-2} and 0.81, respectively, resulting in a PCE of 21.93%. To confirm the superior PCE, steady-state maximum power output (SPO) of the champion device was conducted by fixing the voltage at maximum power point (0.99V) and measuring the photocurrent for about 120 s (Figure 4b). The SPO indicates a stabilized PCE of ~21.6%, close to

the reverse-scan PCE. To verify the J_{SC}, the external quantum efficiency (EQE) was measured and corresponding integrated current-density is plotted in Figure 4c. The J_{SC} from EQE is 23.99 mA·cm^{-2} and only about 0.3 mA cm^{-2} higher than that obtained from the *J-V* curves, which might be due to spectral mismatch. It is worth noting that the devices fabricated by both the low- and high-temperature methods attain their maximum performance after 3-10 days of post-fabrication. While the exact reason behind this remains unclear and outside the scope of this work, an in-depth investigation might be more insightful, especially in the context of understanding why some polycrystalline-based PSCs also exhibit their highest PCE days after their fabrication.[48]

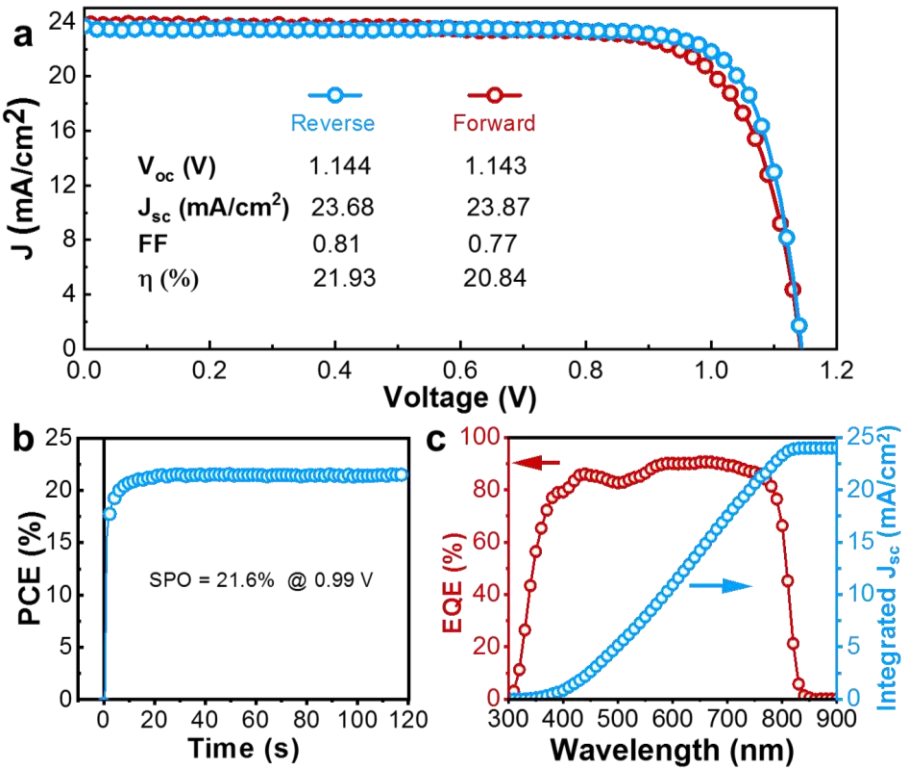

Figure 4. (a) *J*−*V* curves of the champion device under forward(red) and reverse (blue) scans. **(b)** Steady-state PCE output of the champion cell at maximum power point at an applied bias of 0.99 V. **(c)** EQE spectrum and integrated J_{SC} of the champion cell.

In brief, a low-temperature ITC method to grow thin single-crystal films of $MAPbI_3$ was designed via solvent engineering. Compared to high-temperature growth, this approach enhances the film's surface quality and extends the radiative charge carrier lifetime, enabling higher V_{OC} values. SC-PSCs fabricated with this low-temperature method exhibit an enhanced V_{OC} of up to 1.15 V and a champion PCE of 21.93%, which sets a new record for SC-PSCs. With no grain boundaries at play, these results indicate the importance of the surface in advancing perovskite photovoltaic technology, and provides a platform to study PSCs while excluding the effects of grains. Further efforts are needed in evaluating the long-term stability of SC-PSCs under light (for e.g. maximum power point tracking), which calls for the development of proper encapsulation protocols and protection of the interface contacts against external factors such as moisture.[23] Moreover, while the space-limited method produces good-quality films that enable highly-efficient SC-PSCs that are currently appealing for fundamental studies, industrial standards for large-area devices will necessitate the development of more scalable techniques.[49,50] Interface engineering and proper integration of single-crystal films into efficient device architectures will be key for further advancing the performance of SC-PSCs.

ASSOCIATED CONTENT

Details of solution preparation, single-crystal growth, device fabrication and characterization.

AUTHOR INFORMATION

The manuscript was written through contributions of all authors. All authors have approved the final version of the manuscript.

ACKNOWLEDGMENT

The authors acknowledge the funding support from King Abdullah University of Science and Technology (KAUST). The authors thank Prof. Edward H. Sargent for useful discussions and suggestions.

REFERENCES

(1) Best Research-Cell Efficiency Chart | Photovoltaic Research | NREL https://www.nrel.gov/pv/cell-efficiency.html (accessed Nov 20, 2019).
(2) Luo, D.; Su, R.; Zhang, W.; Gong, Q.; Zhu, R. Minimizing Non-Radiative Recombination Losses in Perovskite Solar Cells. *Nat. Rev. Mater.* **2020**, *5* (1), 44–60.
(3) Zheng, X.; Hou, Y.; Bao, C.; Yin, J.; Yuan, F.; Huang, Z.; Song, K.; Liu, J.; Troughton, J.; Gasparini, N.; et al. Managing Grains and Interfaces via Ligand Anchoring Enables 22.3%-Efficiency Inverted Perovskite Solar Cells. *Nat. Energy* **2020**, 1–10, DOI: 10.1038/s41560-019-0538-4
(4) Nie, W.; Tsai, H.; Blancon, J.-C.; Liu, F.; Stoumpos, C. C.; Traore, B.; Kepenekian, M.; Durand, O.; Katan, C.; Tretiak, S.; et al. Critical Role of Interface and Crystallinity on the Performance and Photostability of Perovskite Solar Cell on Nickel Oxide. *Adv. Mater.* **2018**, *30* (5), 1703879.
(5) Zheng, X.; Chen, B.; Dai, J.; Fang, Y.; Bai, Y.; Lin, Y.; Wei, H.; Zeng, X. C.; Huang, J. Defect Passivation in Hybrid Perovskite Solar Cells Using Quaternary Ammonium Halide Anions and Cations. *Nat. Energy* **2017**, *2* (7), 1–9.
(6) Jiang, Q.; Zhao, Y.; Zhang, X.; Yang, X.; Chen, Y.; Chu, Z.; Ye, Q.; Li, X.; Yin, Z.; You, J. Surface Passivation of Perovskite Film for Efficient Solar Cells. *Nat. Photonics* **2019**, *13* (7), 460–466.
(7) Gao, F.; Zhao, Y.; Zhang, X.; You, J. Recent Progresses on Defect Passivation toward Efficient Perovskite Solar Cells. *Adv. Energy Mater.* **2019**, 1902650.
(8) Yang, C.; El-Demellawi, J. K.; Yin, J.; Velusamy, D. B.; Emwas, A.-H. M.; El-Zohry, A. M.; Gereige, I.; AlSaggaf, A.; Bakr, O. M.; Alshareef, H. N.; et al. $MAPbI_3$ Single Crystals Free from Hole-Trapping Centers for Enhanced Photodetectivity. *ACS Energy Lett.* **2019**, *4* (11), 2579–2584.
(9) Quan, L. N.; Rand, B. P.; Friend, R. H.; Mhaisalkar, S. G.; Lee, T.-W.; Sargent, E. H. Perovskites for Next-Generation Optical Sources. *Chem. Rev.* **2019**, *119* (12), 7444–7477.
(10) Stranks, S. D. Nonradiative Losses in Metal Halide Perovskites. *ACS Energy Lett.* **2017**, *2* (7), 1515–1525.
(11) Nie, W.; Tsai, H.; Asadpour, R.; Blancon, J.-C.; Neukirch, A. J.; Gupta, G.; Crochet, J. J.; Chhowalla, M.; Tretiak, S.; Alam, M. A.; et al. High-Efficiency Solution-Processed Perovskite Solar Cells with Millimeter-Scale Grains. *Science* **2015**, *347* (6221), 522–525.
(12) Akin, S.; Arora, N.; Zakeeruddin, S. M.; Grätzel, M.; Friend, R. H.; Dar, M. I. New Strategies for Defect Passivation in High-Efficiency Perovskite Solar Cells. *Adv. Energy Mater.* **2019**, 1903090.
(13) Yoshikawa, K.; Kawasaki, H.; Yoshida, W.; Irie, T.; Konishi, K.; Nakano, K.; Uto, T.; Adachi, D.; Kanematsu, M.; Uzu, H.; et al. Silicon Heterojunction Solar Cell with Interdigitated Back Contacts for a Photoconversion Efficiency over 26%. *Nat. Energy* **2017**, *2* (5), 1–8.

(14) Aberle, A. G. Surface Passivation of Crystalline Silicon Solar Cells: A Review. *Prog. Photovolt. Res. Appl.* **2000**, *8* (5), 473–487.
(15) Zhao, J.; Wang, A.; Green, M. A.; Ferrazza, F. 19.8% Efficient "Honeycomb" Textured Multicrystalline and 24.4% Monocrystalline Silicon Solar Cells. *Appl. Phys. Lett.* **1998**, *73* (14), 1991–1993.
(16) Shi, D.; Adinolfi, V.; Comin, R.; Yuan, M.; Alarousu, E.; Buin, A.; Chen, Y.; Hoogland, S.; Rothenberger, A.; Katsiev, K.; et al. Low Trap-State Density and Long Carrier Diffusion in Organolead Trihalide Perovskite Single Crystals. *Science* **2015**, *347* (6221), 519–522.
(17) Dong, Q.; Fang, Y.; Shao, Y.; Mulligan, P.; Qiu, J.; Cao, L.; Huang, J. Electron-Hole Diffusion Lengths >175 μm in Solution-Grown $CH_3NH_3PbI_3$ Single Crystals. *Science* **2015**, *347* (6225), 967–970.
(18) Liu, Y.; Zhang, Y.; Yang, Z.; Feng, J.; Xu, Z.; Li, Q.; Hu, M.; Ye, H.; Zhang, X.; Liu, M.; et al. Low-Temperature-Gradient Crystallization for Multi-Inch High-Quality Perovskite Single Crystals for Record Performance Photodetectors. *Mater. Today* **2019**, *22*, 67–75.
(19) Alarousu, E.; El-Zohry, A. M.; Yin, J.; Zhumekenov, A. A.; Yang, C.; Alhabshi, E.; Gereige, I.; AlSaggaf, A.; Malko, A. V.; Bakr, O. M.; et al. Ultralong Radiative States in Hybrid Perovskite Crystals: Compositions for Submillimeter Diffusion Lengths. *J. Phys. Chem. Lett.* **2017**, *8* (18), 4386–4390.
(20) Fang, H.-H.; Raissa, R.; Abdu-Aguye, M.; Adjokatse, S.; Blake, G. R.; Even, J.; Loi, M. A. Photophysics of Organic–Inorganic Hybrid Lead Iodide Perovskite Single Crystals. *Adv. Funct. Mater.* **2015**, *25* (16), 2378–2385.
(21) Zhumekenov, A. A.; Saidaminov, M. I.; Haque, M. A.; Alarousu, E.; Sarmah, S. P.; Murali, B.; Dursun, I.; Miao, X.-H.; Abdelhady, A. L.; Wu, T.; et al. Formamidinium Lead Halide Perovskite Crystals with Unprecedented Long Carrier Dynamics and Diffusion Length. *ACS Energy Lett.* **2016**, *1* (1), 32–37.
(22) Murali, B.; Kolli, H. K.; Yin, J.; Ketavath, R.; Bakr, O. M.; Mohammed, O. F. Single Crystals: The Next Big Wave of Perovskite Optoelectronics. *ACS Mater. Lett.* **2019**, 184–214.
(23) Chen, Z.; Turedi, B.; Alsalloum, A. Y.; Yang, C.; Zheng, X.; Gereige, I.; AlSaggaf, A.; Mohammed, O. F.; Bakr, O. M. Single-Crystal MAPbI3 Perovskite Solar Cells Exceeding 21% Power Conversion Efficiency. *ACS Energy Lett.* **2019**, *4* (6), 1258–1259.
(24) Hutter, E. M.; Gélvez-Rueda, M. C.; Osherov, A.; Bulović, V.; Grozema, F. C.; Stranks, S. D.; Savenije, T. J. Direct–Indirect Character of the Bandgap in Methylammonium Lead Iodide Perovskite. *Nat. Mater.* **2017**, *16* (1), 115–120.
(25) Chen, Z.; Dong, Q.; Liu, Y.; Bao, C.; Fang, Y.; Lin, Y.; Tang, S.; Wang, Q.; Xiao, X.; Bai, Y.; et al. Thin Single Crystal Perovskite Solar Cells to Harvest Below-Bandgap Light Absorption. *Nat. Commun.* **2017**, *8* (1), 1890.
(26) Wang, T.; Daiber, B.; Frost, J. M.; Mann, S. A.; Garnett, E. C.; Walsh, A.; Ehrler, B. Indirect to Direct Bandgap Transition in Methylammonium Lead Halide Perovskite. *Energy Environ. Sci.* **2017**, *10* (2), 509–515.
(27) Wang, K.; Yang, D.; Wu, C.; Shapter, J.; Priya, S. Mono-Crystalline Perovskite Photovoltaics toward Ultrahigh Efficiency? *Joule* **2019**, *3* (2), 311–316.
(28) Cheng, X.; Yang, S.; Cao, B.; Tao, X.; Chen, Z. Single Crystal Perovskite Solar Cells: Development and Perspectives. *Adv. Funct. Mater.* **2019**, 1905021.

(29) Liu, Y.; Zhang, Y.; Yang, Z.; Yang, D.; Ren, X.; Pang, L.; Liu, S. (Frank). Thinness- and Shape-Controlled Growth for Ultrathin Single-Crystalline Perovskite Wafers for Mass Production of Superior Photoelectronic Devices. *Adv. Mater.* **2016**, *28* (41), 9204–9209.
(30) Saidaminov, M. I.; Abdelhady, A. L.; Murali, B.; Alarousu, E.; Burlakov, V. M.; Peng, W.; Dursun, I.; Wang, L.; He, Y.; Maculan, G.; et al. High-Quality Bulk Hybrid Perovskite Single Crystals within Minutes by Inverse Temperature Crystallization. *Nat. Commun.* **2015**, *6* (1), 1–6.
(31) Fan, Z.; Xiao, H.; Wang, Y.; Zhao, Z.; Lin, Z.; Cheng, H.-C.; Lee, S.-J.; Wang, G.; Feng, Z.; Goddard, W. A.; et al. Layer-by-Layer Degradation of Methylammonium Lead Tri-Iodide Perovskite Microplates. *Joule* **2017**, *1* (3), 548–562.
(32) Chen, L.-C.; Chen, C.-C.; Chen, J.-C.; Wu, C.-G. Annealing Effects on High-Performance $CH_3NH_3PbI_3$ Perovskite Solar Cells Prepared by Solution-Process. *Sol. Energy* **2015**, *122*, 1047–1051.
(33) Yang, Y.; Yang, M.; Moore, D. T.; Yan, Y.; Miller, E. M.; Zhu, K.; Beard, M. C. Top and Bottom Surfaces Limit Carrier Lifetime in Lead Iodide Perovskite Films. *Nat. Energy* **2017**, *2* (2), 1–7.
(34) Zhumekenov, A. A.; Haque, M. A.; Yin, J.; El-Zohry, A. M.; Lee, K. J.; Dursun, I.; Mohammed, O. F.; Baran, D.; Bakr, O. M. Reduced Ion Migration and Enhanced Photoresponse in Cuboid Crystals of Methylammonium Lead Iodide Perovskite. *J. Phys. Appl. Phys.* **2018**, *52* (5), 054001.
(35) Han, G.; Koh, T. M.; Lim, S. S.; Goh, T. W.; Guo, X.; Leow, S. W.; Begum, R.; Sum, T. C.; Mathews, N.; Mhaisalkar, S. Facile Method to Reduce Surface Defects and Trap Densities in Perovskite Photovoltaics. *ACS Appl. Mater. Interfaces* **2017**, *9* (25), 21292–21297.
(36) Hamill, J. C.; Schwartz, J.; Loo, Y.-L. Influence of Solvent Coordination on Hybrid Organic–Inorganic Perovskite Formation. *ACS Energy Lett.* **2018**, *3* (1), 92–97.
(37) Nayak, P. K.; Moore, D. T.; Wenger, B.; Nayak, S.; Haghighirad, A. A.; Fineberg, A.; Noel, N. K.; Reid, O. G.; Rumbles, G.; Kukura, P.; et al. Mechanism for Rapid Growth of Organic–Inorganic Halide Perovskite Crystals. *Nat. Commun.* **2016**, *7* (1), 1–8.
(38) Mammana, S. S.; Greatti, A.; Luiz, F. H.; da Costa, F. I.; Mammana, A. P.; Calligaris, G. A.; Cardoso, L. P.; Mammana, C. I. Z.; den Engelsen, D. Study of Wet Etching Thin Films of Indium Tin Oxide in Oxalic Acid by Monitoring the Resistance. *Thin Solid Films* **2014**, *567*, 20–31.
(39) Murali, B.; Yengel, E.; Yang, C.; Peng, W.; Alarousu, E.; Bakr, O. M.; Mohammed, O. F. The Surface of Hybrid Perovskite Crystals: A Boon or Bane. *ACS Energy Lett.* **2017**, *2* (4), 846–856.
(40) Luo, D.; Yang, W.; Wang, Z.; Sadhanala, A.; Hu, Q.; Su, R.; Shivanna, R.; Trindade, G. F.; Watts, J. F.; Xu, Z.; et al. Enhanced Photovoltage for Inverted Planar Heterojunction Perovskite Solar Cells. *Science* **2018**, *360* (6396), 1442–1446.
(41) Zheng, X.; Troughton, J.; Gasparini, N.; Lin, Y.; Wei, M.; Hou, Y.; Liu, J.; Song, K.; Chen, Z.; Yang, C.; et al. Quantum Dots Supply Bulk- and Surface-Passivation Agents for Efficient and Stable Perovskite Solar Cells. *Joule* **2019**, *3* (8), 1963–1976.
(42) De Marco, N.; Zhou, H.; Chen, Q.; Sun, P.; Liu, Z.; Meng, L.; Yao, E.-P.; Liu, Y.; Schiffer, A.; Yang, Y. Guanidinium: A Route to Enhanced Carrier Lifetime and Open-Circuit Voltage in Hybrid Perovskite Solar Cells. *Nano Lett.* **2016**, *16* (2), 1009–1016.

(43) Wetzelaer, G.-J. A. H.; Scheepers, M.; Sempere, A. M.; Momblona, C.; Ávila, J.; Bolink, H. J. Trap-Assisted Non-Radiative Recombination in Organic–Inorganic Perovskite Solar Cells. *Adv. Mater.* **2015**, *27* (11), 1837–1841.
(44) Stolterfoht, M.; Caprioglio, P.; Wolff, C. M.; Márquez, J. A.; Nordmann, J.; Zhang, S.; Rothhardt, D.; Hörmann, U.; Amir, Y.; Redinger, A.; et al. The Impact of Energy Alignment and Interfacial Recombination on the Internal and External Open-Circuit Voltage of Perovskite Solar Cells. *Energy Environ. Sci.* **2019**, *12* (9), 2778–2788.
(45) Dar, M. I.; Franckevičius, M.; Arora, N.; Redeckas, K.; Vengris, M.; Gulbinas, V.; Zakeeruddin, S. M.; Grätzel, M. High Photovoltage in Perovskite Solar Cells: New Physical Insights from the Ultrafast Transient Absorption Spectroscopy. *Chem. Phys. Lett.* **2017**, *683*, 211–215.
(46) Stolterfoht, M.; Wolff, C. M.; Márquez, J. A.; Zhang, S.; Hages, C. J.; Rothhardt, D.; Albrecht, S.; Burn, P. L.; Meredith, P.; Unold, T.; et al. Visualization and Suppression of Interfacial Recombination for High-Efficiency Large-Area Pin Perovskite Solar Cells. *Nat. Energy* **2018**, *3* (10), 847–854.
(47) Wolff, C. M.; Caprioglio, P.; Stolterfoht, M.; Neher, D. Nonradiative Recombination in Perovskite Solar Cells: The Role of Interfaces. *Adv. Mater.* **2019**, *31* (52), 1902762.
(48) Saliba, M.; Correa-Baena, J.-P.; Wolff, C. M.; Stolterfoht, M.; Phung, N.; Albrecht, S.; Neher, D.; Abate, A. How to Make over 20% Efficient Perovskite Solar Cells in Regular (n–i–p) and Inverted (p–i–n) Architectures. *Chem. Mater.* **2018**, *30* (13), 4193–4201.
(49) Liu, Y.; Ren, X.; Zhang, J.; Yang, Z.; Yang, D.; Yu, F.; Sun, J.; Zhao, C.; Yao, Z.; Wang, B.; et al. 120 mm Single-Crystalline Perovskite and Wafers: Towards Viable Applications. *Sci. China Chem.* **2017**, *60* (10), 1367–1376.
(50) Wang, X.-D.; Li, W.-G.; Liao, J.-F.; Kuang, D.-B. Recent Advances in Halide Perovskite Single-Crystal Thin Films: Fabrication Methods and Optoelectronic Applications. *Sol. RRL* **2019**, *3* (4), 1800294.